

Topological Statistics and the LMT Galaxy Redshift Project

Dimitris Mitsouras¹, Robert Brandenberger^{2,3} and Paul Hickson³

¹*Computer Science Department, Brown University, Providence, R.I. 02912, USA*

²*Physics Department, Brown University, Providence, R.I. 02912, USA*

³*Department of Physics and Astronomy, University of British Columbia, Vancouver, B.C. V6T 1Z1, CANADA*

7 May 2018

ABSTRACT

The results of numerical simulations are presented which demonstrate that liquid mirror telescope galaxy redshift surveys such as the current UBC-NASA Multi-Narrowband Survey and the future LZT Survey have the potential of discriminating between the predictions of different theories of structure formation. Most of the currently studied theories of structure formation predict a scale-invariant spectrum of primordial perturbations. Therefore, to distinguish between the predictions of the various models, we make use of statistics which are sensitive to non-Gaussian phases, such as the counts in cell statistics, N-galaxy probability functions and Minkowski functionals. It is shown that already the current UBC-NASA survey can clearly differentiate between the predictions of some topological defect theories and those of inflationary Universe models with Gaussian phases.

Key words: cosmology: theory – large-scale structure, redshift surveys

BROWN-HET-1116

April 1998.

1 INTRODUCTION

Liquid mirror telescope (LMT) redshift surveys provide an efficient way to study the distribution of galaxies in the Universe. Recent technological developments at Laval University and the University of British Columbia (Borra et al. 1992, Hickson et al. 1994) have made liquid mirrors a viable low-cost alternative to glass mirrors for zenith-pointing telescopes. These surveys employ a set of medium-band filters to measure the spectral energy distributions (SEDs) of every detectable object in a long strip of sky a few tenths of a degree wide. From the SEDs, galaxy types and redshifts are estimated by fitting spectral templates to the data. The resulting redshifts have typical redshift accuracy of order 0.01 - 0.03 depending on the wavelength coverage and signal-to-noise ratio (Hickson, Gibson and Callaghan 1994). The technique is similar to that of photometric redshifts derived from broad-band filters (eg. Koo 1985, Lanzetta et al 1996) but provides about an order of magnitude improvement in redshift accuracy for the same signal-to-noise ratio. A first such survey, the UBC-NASA Multi-Narrowband survey (Hickson & Mulrooney, 1998), is nearing its completion, and a new larger-scale project, the LZT survey, which will probe the Universe to a much greater depth, is in construction.

The 6-m Large Zenith Telescope (LZT) (Hickson et al. 1998) is expected to provide redshifts for galaxies as faint as 23rd magnitude. This is several magnitudes fainter than can be reached by current and planned wide-angle spectroscopic surveys such as the 2DF (Maddox 1998) and Sloan Digital Sky Survey. However, the photometrically derived redshifts of the UBC-NASA survey and future LZT are less accurate than spectroscopic redshifts.

The goal of this study is to determine if, in spite of the substantial redshift errors and of the narrow-strip geometry of the survey region, liquid mirror galaxy redshift surveys have the potential to reveal important information about the origin of structure in the Universe. Specifically, we are interested in exploring whether the surveys can distinguish between the predictions of models of structure formation which are characterized by the same primordial power spectrum of mass fluctuations, but which have different phase relations, e.g. on one hand inflationary Universe models with Gaussian random phases, and on the other hand topological defect theories characterized by rich nontrivial phase correlations.

A second goal of this study is to explore which aspects of the technology future improvement should focus on if the goal of the survey is to gain more information about the origin of structure in the Universe. Specifically, what does one gain by increasing the depth of the survey compared

to what one would gain by increasing the accuracy of the redshifts by adding more filters.

We study these issues by performing numerical simulations of various theories of structure formation, slicing from the simulation box regions with the geometry of the LMT surveys, and analyzing the results using statistical measures which are sensitive to a non-Gaussian distribution of phases. Specifically, we shall evaluate counts-in-cell (CIC) statistics, N-galaxy probability functions (NPF) and Minkowski functionals (Mecke et al. 1994).

We compare the results of inflation-based cold dark matter (CDM) theories and topological defect models. Since the dynamics of actual defect models is very complicated and not yet completely understood, we will investigate toy model realizations constructed to maximize the degree of non-Gaussianness. We study cosmic string and global texture models (a global monopole theory would be rather similar to the texture model). For strings, we study two extreme versions of the theory. The first is a “filament” model which is realized if the strings have a lot of small-scale structure and therefore are characterized by a small transverse velocity, leading to a filamentary pattern of accretion. The second is a “wake” model which is realistic if the strings have little small-scale structure, large transverse velocity, and no local gravitational potential, and thus lead to planar velocity perturbations in their wake.

Our simulations demonstrate that already with the current UBC-NASA survey useful lessons for cosmology can be deduced. With a limiting magnitude (AB magnitude scale) of 20.4 and galaxy redshift errors of $\Delta z < 0.03$ (based on the use of 33 filters), the complete survey will allow us to differentiate between the predictions of idealized defect theories and Gaussian models. With an improvement of the redshift errors and survey depth which will be possible with the LZT survey, the distinguishing power of the survey will be greatly increased.

2 MODELS

Standard Cold Dark Matter Model

There are two main classes of theories of structure formation which have been investigated over the past decade. The first are inflation-based models with a scale-invariant spectrum of primordial adiabatic perturbations with random phases, each having a Gaussian distribution. These models are viable only if the dark matter is cold (resulting in the so-called *Cold Dark Matter* (CDM) models). In this paper, we shall study the “standard” CDM model with an exactly scale-invariant spectrum of perturbations, $\Omega = 1$, and vanishing cosmological constant. This specific model is no longer viable if we compare the normalization of the power spectrum of density perturbations with that of CMB fluctuations. Viable CDM models either require an admixture of hot dark matter, a value of Ω smaller than one, a remnant cosmological constant contributing significantly to Ω , or a tilt of the primordial spectrum of perturbations. However, in this paper we are mostly concerned with the power of the LMT surveys to pick up signatures of primordial non-random phases, and the model we study is taken as the canonical model with Gaussian random phases.

Thus, we consider a CDM model with $\Omega = 1$, $h = 0.5$,

with vanishing cosmological constant, and having an exactly scale-invariant primordial spectrum of cosmological perturbations (generated as quantum fluctuations in an early period of inflation (Chibisov & Mukhanov 1980, Chibisov & Mukhanov 1982, Lukash 1980, Mukhanov & Chibisov 1981, Guth & Pi 1982, Hawking 1982, Starobinskii 1982, Bardeen et al. 1983). The processing of the primordial spectrum of perturbations at late times on scales smaller than the Hubble radius leads to a nontrivial transfer function. We take the transfer function given in Bardeen et al. (1986).

A cosmological model with these parameters was evolved numerically in a box of comoving length of 700Mpc with 128^3 particles. The normalization of the primordial power spectrum was chosen such that $\sigma_8 = 0.95$ (note that a COBE normalized model would require $\sigma_8 = 1.22$). The numerical work was done with the Bertschinger & Gelb (1991) P^3M N-body code and was run on the CRAY-YMP at the Brown Center for Scientific Computation.

String Wake Model

The second class of structure formation models which has received a lot of attention over the past decade is based on topological defects giving rise to the seeds for structures (see Vilenkin & Shellard (1994), Hindmarsh & Kibble (1995) or Brandenberger (1994) for recent reviews). Models based on strings, global monopoles, and textures are of special interest (models with local monopoles or domain walls are ruled out since the defects in these models would overclose the Universe).

Topological defects are a generic prediction of a wide class of particle physics models. If the set of vacuum states of the theory after symmetry breaking has a nontrivial topology, then defects will inevitably be produced during the symmetry breaking phase transition in the early Universe (Kibble 1976). The defects form non-adiabatic density perturbations and act as the seeds of structure formation. If the scale of symmetry breaking is about 10^{16} GeV, then the resulting spectrum of perturbations has the correct amplitude to explain the large-scale fluctuations in the cosmic microwave background observed by COBE (Smoot et al. 1992).

Cosmic strings are linear topological defects which arise if the vacuum manifold of the particle physics theory is not simply connected. At the time of the phase transition, a network of strings is formed. The strings are either infinite in length or closed loops. The *long* string network consists of all the strings whose curvature radius is greater than the Hubble radius. Causality considerations show that the correlation length $\xi(t)$ of the long string network (the mean separation of the long strings) must be smaller or equal to the Hubble radius at all times after the phase transition. Analytical arguments (Vilenkin 1985) and numerical studies (Albrecht & Turok 1989, Bennett & Bouchet 1988, Allen & Shellard 1990) demonstrate that the string network takes on a *scaling solution* in which $\xi(t) \sim t$ for all t . Hence, it follows that the cosmic string model predicts a scale-invariant spectrum of primordial perturbations, much like inflationary Universe models. In contrast to the latter, however, the phases of the perturbations in the string model are non-random.

The precise nature of the non-random phases (more specifically the topology of the dominant structures produced in the cosmic string model) depend on some details of the string dynamics which are, unfortunately, not yet re-

solved. If the strings are straight on the scale of the Hubble radius, then the string tension will equal the mass per unit length μ . As a consequence, the strings will move relativistically, and they exert no local gravitational force. In contrast, if the long strings have a lot of small-scale structure, then the tension will be smaller than μ , the transverse motion of the strings will be slower and there will be a local gravitational force exerted by the strings. The first scenario gives rise to the *cosmic string wake model*, the second to the *cosmic string filament model*.

Note that since the strings are non-adiabatic seed perturbations, then, in a model in which the dark matter is hot, free streaming does not erase the primordial perturbations on small scales. Hence, the cosmic string model of structure formation is viable even if the dark matter is hot (Vilenkin & Shafi 1983, Brandenberger et al. 1987a, 1987b).

A straight cosmic string without small-scale structure generates a conical space perpendicular to the string with deficit angle (Vilenkin 1981)

$$\alpha = 8\pi G\mu \quad (1)$$

(We use units in which the speed of light $c = 1$). If the string is moving through a plasma with transverse velocity v , this induces a velocity perturbation (Silk & Vilenkin 1984) of magnitude

$$\delta v = 4\pi G\mu\gamma(v), \quad (2)$$

where $\gamma(v)$ is the relativistic γ factor associated with the velocity v . The velocity perturbations, in turn, leads to a non-adiabatic density perturbation of roughly planar geometry - a wake. The dimensions of the plane are determined by the string velocity v and by the correlation length $\xi(t)$. A string at time t_i produces a wake of comoving length $v\xi(t_i)z(t_i)$ and width $\xi(t_i)z(t_i)$. The wake thickness can be calculated (Perivolaropoulos et al. 1990, Brandenberger 1991) using the Zel'dovich approximation (Zel'dovich 1970) as the comoving scale of the region which has separated from the Hubble flow and is no longer expanding. Because of free streaming, the result depends on the nature of the dark matter. For hot dark matter, the thickness at the present time t_0 of a wake created at time $t_i > t_{eq}$ is (Perivolaropoulos et al. 1990, Brandenberger 1991)

$$h(t_i) = \frac{24\pi}{5} G\mu v\gamma(v)z(t_i)^{1/2}t_0. \quad (3)$$

Thus, the wake dimensions are

$$v\xi(t_i)z(t_i) \times \xi(t_i)z(t_i) \times h(t_i). \quad (4)$$

The mass of such a structure is

$$m(t_i) = \frac{24\pi}{5} G\mu v^2\gamma(v)\nu_1^{-2}\rho_0 t_i^{1/3}t_0^{8/3}, \quad (5)$$

where we have taken the string correlation length to be $\xi(t) = \frac{1}{\nu_1}t$.

Hot dark matter wakes created before the time t_{eq} of equal matter and radiation are diluted by the radiation pressure and will not be included in our simulations. Note that in the cosmic string wake model, the structures which dominate the large-scale distribution of galaxies are predicted to be planar wakes. The most numerous and thickest are those created at t_{eq} . Their size is comparable to that of the Great Wall (de Lapparent et al. 1986).

The procedure for setting up a toy wake model simulation is the following. The time interval between t_{eq} and t_0 is divided into Hubble times. For the cosmological parameters used in this paper, there are 16 Hubble time steps. At each time step, labeled by a time t_i , a number c_w^{-3} of wakes are laid down per volume t_i^3 . Here, $c_w t_i$ gives the mean separation of wakes at this time. Wakes are laid down by selecting centers and orientations of the wakes at random within each volume t_i^3 . For given values of $G\mu$, of the mean transverse velocity of the string v and of the number ν_1 , the value of c_w can be determined by demanding that the total mass density adds up to critical density.

In principle, the number ν_1 could be determined by numerical simulations. In practice, however, the resolution of the cosmic string evolution codes may not be good enough to give a reliable answer. Thus, we will consider a range of values. To be specific, we choose the following values: $G\mu = 10^{-6}$, $v\gamma(v) = 1$ and ν_1 .

Given the geometrical distribution of wakes, galaxies are laid down at random within the volume of the wakes, with a uniform density.

String Filament Model

Long cosmic strings with a substantial amount of small-scale structure (e.g. small-scale wiggles) will have a coarse-grained equation of state which differs from that of a relativistic string, i.e. $|p| < \mu$, where $|p|$ denotes the string tension. In this case, the strings will have a small transverse velocity, but they will exert a local gravitational attraction, and hence they will seed filamentary density perturbations. We shall take the extreme situation in which the transverse string velocity is negligible (the intermediate case was analyzed in Zanchin et al. (1996)). In this case, the comoving radius $q_{nl}(t_i)$ of a filament seeded at time t_i can again be calculated using the Zel'dovich approximation, yielding (Aguirre & Brandenberger 1995)

$$q_{nl}(t_i) = \left(\frac{12G\lambda}{5}\ln\left(\frac{t_0}{t_i}\right)\right)^{1/2}t_0, \quad (6)$$

where $\lambda = \mu - |p|$. Hence, the mass in an individual filament which was seeded at time t_i is

$$m(t_i) = \frac{12\pi G\lambda}{5}\frac{1}{\nu_1}\rho_0 t_0^{8/3}t_i^{1/3}\ln\left(\frac{t_0}{t_i}\right), \quad (7)$$

where ν_1 is defined as in the previous subsection.

The procedure for setting up the string filament simulation is analogous to how the wake toy model is constructed. At each Hubble time step between t_{eq} and t_0 , a fixed number c_f^{-3} of filaments for volume t^3 is laid down, choosing filament centers and directions at random. For given values of $G\lambda$ and ν_1 , the number of filaments is determined by demanding that the total mass adds up to critical density. Galaxies are again put down at random in the volume of the filaments, with a uniform density. To be specific, we shall consider the values $G\lambda = 10^{-6}$ and $\nu_1 = 1$.

Note that the string filament and string wake models represent opposite extremes of what we expect a realistic string model to look like. The statistical study of the wake and filament models will hence yield as a byproduct a quantitative measure of the large uncertainty in the predictions of the string model, in particular if we let ν_1 vary over a significant range of values.

Texture Model

Textures (Davis 1987) are topological defects which

arise if the vacuum manifold of the particle physics model has nontrivial third homotopy group. In four space-time dimensions, textures are unstable (Turok 1989). Texture configurations on Hubble scale unwind within approximately one Hubble expansion time. Nevertheless, in theories with a global symmetry, textures are able to generate density perturbations. In field theories with a local symmetry, texture configurations in the scalar matter fields can be compensated by gauge fields on a microscopic time scale, and hence in such models textures are not important for structure formation.

The simplest texture configurations (Turok 1989) are spherically symmetric. Hence, we will construct a texture toy model by superimposing individual spherically symmetric texture configurations. Obviously, this is a gross simplification of what a texture model will really look like.

At each time t_i , there is a finite probability (Prokopec 1991, Leese and Prokopec 1991) p that in a volume t_i^3 there will be a texture configuration. The initial texture configuration can be modeled (Gooding et al. 1991) by a spherically symmetric velocity perturbation which then develops into a spherically symmetric density perturbations. The comoving radius $q_{nl}(t_i)$ of this perturbation can again be determined (Aguirre 1995) by the Zel'dovich approximation, yielding the result

$$q_{nl}(t_i) = \frac{6}{5} \epsilon t_i^{-1/3} t_0^{4/3}, \quad (8)$$

where (up to factors of order unity) $\epsilon = G\eta^2$, η being the scale of symmetry breaking. We will take the value $\epsilon = 3 \times 10^{-5}$, an appropriate value for a COBE-normalized texture model (Pen et al. 1997). The mass in a texture can be computed by multiplying the volume of the texture by the background density.

The texture toy model was obtained by laying down p texture centers per volume t_i^3 at each Hubble expansion time t_i with a random choice of the centers. Galaxies were distributed within each texture with a Gaussian density profile (as a function of radius) and random angular distribution. To agree with the total mass obtained in the other toy models, the number of galaxies per texture was chosen to (for fixed values of ϵ and p) yield critical density for the entire volume.

General Comments

Note that all four models discussed above predict a roughly scale-invariant primordial spectrum of perturbations. In the case of inflation, the reason for the scale invariance can be explained by the basic geometry of an inflationary cosmology (see e.g. Press (1980) or Brandenberger (1985)), in defect models the approximate scale-invariance is a direct consequence of the scaling dynamics of the defect system (see e.g. Brandenberger (1994)). However, the morphology in these four models is very different, and with the statistics discussed below we are able to differentiate between their predictions for the large-scale structure of the Universe.

3 STATISTICS

Counts in Cell Statistic

The first statistic evaluated for our simulations was a simple *counts in cell* (CIC) statistic (see e.g. Saslaw (1989)).

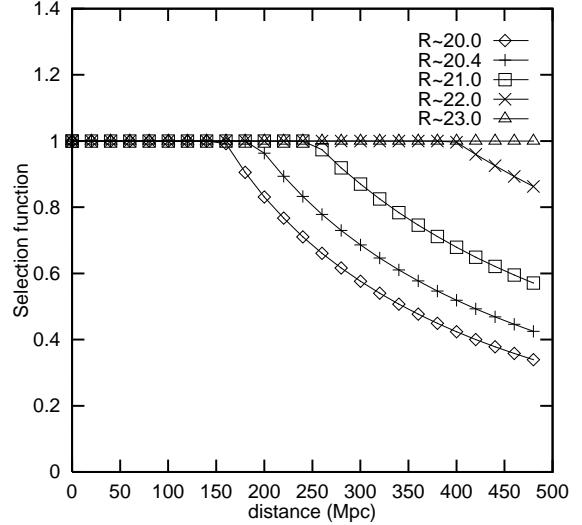


Figure 1. The LMT selection function for various values of the limiting magnitude.

Each LMT slice was projected into a two-dimensional plane and then divided into equal volume cells (three-dimensional volume). An equal number of cells in radial and angular direction was chosen. Note that the shape of the cells depends strongly on the redshift, i.e. the cells are not isometric. However, since we are comparing the predictions of different models (and eventually with observations) all treated the same way, the unusual cell shape distribution should not be a problem.

The CIC statistic is a histogram of number of cells with n galaxies as a function of the number n . The CIC statistic can be evaluated for any cell size (smoothing length). Since the difference in the predictions of the models is expected to be most important on scales slightly less than the size of the dominant structures expected in our models, i.e. of comoving length scale $t_{eq}z(t_{eq})$, a smoothing length comparable to this scale must be chosen. We took 34 cells per side which corresponds to a cell length of about $15h^{-1}$ Mpc.

N-Galaxy Probability Function

The second measure we used is the N-galaxy probability function (NPF), a generalization of the void probability function (Hamilton et al. 1985). The NPF (Aguirre 1995) of a galaxy distribution is the probability that there are exactly N galaxies in a randomly placed volume V , considered as a function of V . Instead of plotting the NPF's, we have found it more informative to plot the cumulative NPF, which for fixed value of N is the probability that there are less than or equal to N galaxies within a randomly placed volume V .

Minkowski Functionals

The Minkowski functionals (Mecke and Wagner 1991) supply a complete characterization of the global morphology of an a galaxy distribution. Given an isodensity surface ∂K in three spatial dimensions, the morphology is determined by four quantities. The first functional M_0 is the volume V enclosed by the surface

$$M_0 = V, \quad (9)$$

the second is related to the surface area A

$$M_1 = A/8, \quad (10)$$

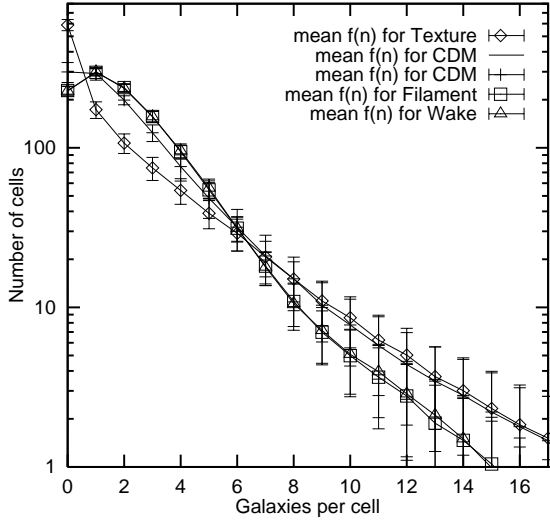


Figure 2. The CIC statistic applied to the LMT geometry for simulations of the standard CDM model, the texture toy model, and the string wake and filament toy models. Redshift error $\Delta z = 0.03$ and limiting magnitude $R = 20.4$ correspond to the values of the current UBC-NASA survey.

the third is proportional to the integrated mean curvature H

$$M_2 = \frac{1}{2\pi^2} H \quad (11)$$

with

$$H = \frac{1}{2} \int_{\partial K} dA \left(\frac{1}{R_1} + \frac{1}{R_2} \right) \quad (12)$$

where R_1 and R_2 are the principal curvature radii of the surface. Finally, the fourth Minkowski functional is related to the Euler characteristic χ and hence to the genus

$$M_3 = \frac{3\chi}{4\pi}, \quad (13)$$

where

$$\chi = \int_{\partial K} dA \frac{1}{R_1 R_2}. \quad (14)$$

There are many ways of displaying the Minkowski functionals as a function for the density contrast. We use the method of Mecke et al. (1994) and Kerscher et al. (1997) and display the functionals as a function of a length scale r . Given a value of r , we consider a volume made up of the union of balls of radii r whose centers are the galaxies in our sample. Note that r play the role of a neighborhood relation length and is similar to a smoothing length of the density field. The larger the value of r , the smaller is the value of the density contrast whose isodensity surface the Minkowski functionals are describing. We made use of modified versions of codes to evaluate the Minkowski functionals made available by Kerscher et al. (1997) and Schmalzing & Buchert (1997), which include boundary corrections.

4 SIMULATIONS AND RESULTS

Our analysis is done in the following way. A simulation of each of the models discussed in Section 2 is performed in a

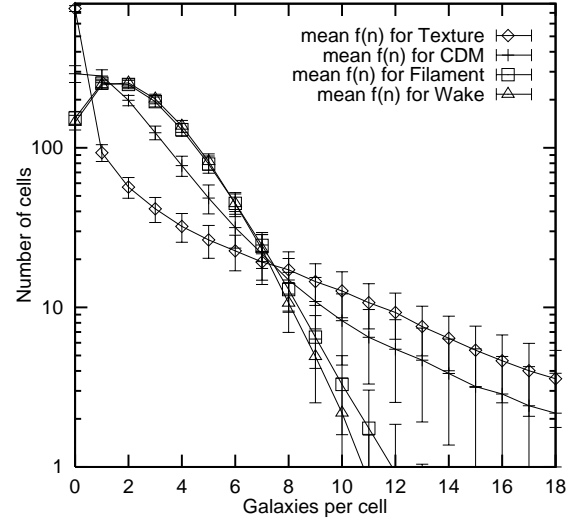


Figure 3. Same as Figure 2, but for a survey with smaller redshift errors of $\Delta z = 0.01$.

box of side length $700h^{-1}$ Mpc. Next, a slice with the geometry of the LMT survey (90° in length and 0.26° in width) is cut out of this box. The slice has a depth of $500h^{-1}$ Mpc. Thus, in order to compare observational results to the simulations, a volume limited subset of the observational data must be used.

To compare the simulations with a survey with a limiting apparent magnitude m_{limit} , particles from the simulations are picked at random using a selection function $s(d)$, where d is the distance from the origin. The selection function was determined by assuming a Press-Schechter luminosity function

$$f(L) = c \left(\frac{L}{L^*} \right)^\alpha e^{-L/L^*} \quad (15)$$

where L stands for the luminosity and c is a constant which drops out of the analysis. The value of L^* was taken (Zucca et al. 1997) to correspond to the absolute magnitude $M^* = -19.6 + 5 \log h$, and a value of $\alpha = -1.22$ appropriate for field galaxies was chosen. A sharp lower cutoff on this luminosity function at a value corresponding to $M = -16$ was used. The resulting selection function is shown in Figure 1 for various values of the limiting apparent magnitude.

To mimic the redshift errors expected in the LMT survey, each galaxy was moved in redshift direction by a redshift error chosen from a Gaussian distribution with standard deviation Δz . For a fixed box, the processes of picking an LMT slice, selecting galaxies and moving their redshifts randomly as described above was repeated many times. For the CIC and NPF graphs, the results are based on 6 slices, each randomized 100 times. For the Minkowski functional graphs, only 10 randomizations for each of the 6 slices was used. The error bars shown on the graphs displaying our results for the CIC and NPF statistics represent the standard deviation resulting from this procedure and not the standard deviation of the mean. The reason for this choice is that, since only one data slice will be available, the error in the observations will be approximated by the standard deviation of a single simulation rather than by the standard deviation of the mean.

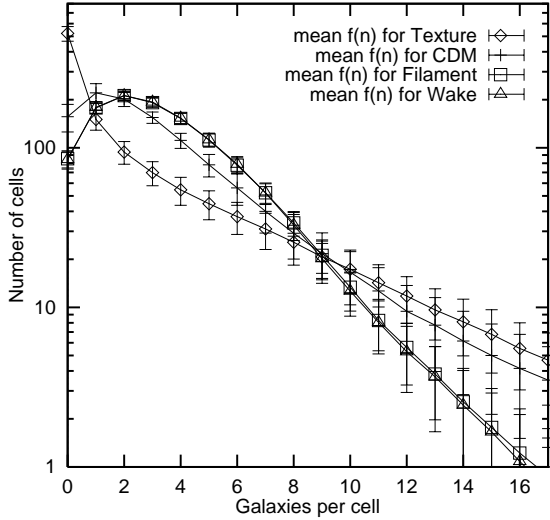


Figure 4. Same as Figure 2, but for a survey with a greater limiting magnitude of $R = 23$.

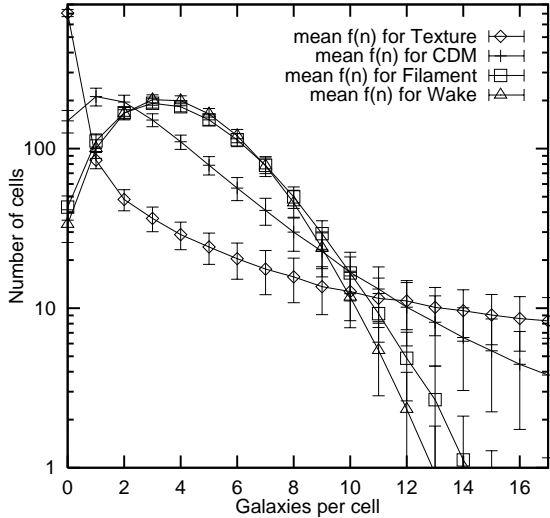


Figure 5. Same as Figure 2, but for the specifications of the LZT survey ($\Delta z = 0.01$ and $R = 23$).

Figures 2 - 7 depict the CIC statistic for the four models studied in this paper. Figure 2 shows the results for the limiting magnitude and redshift errors which are realized in the prototype UBC-NASA Multi-Narrowband Survey: $R = 20.4$ and $\Delta z = 0.03$. Focusing on the region corresponding to a low number of galaxies per cell, it is clear that already this prototype experiment can yield first results of interest to cosmology. A cosmological model like the texture toy model can be clearly differentiated from string models and from a standard CDM theory. The difference between the string and CDM models, however, is not significant. The basic reason why already the prototype survey will be able to distinguish between the most extreme version of large-scale structure formation models is because the redshift error corresponds to a distance smaller than the separation of the dominant structures in our models, which is the comoving Hubble radius at t_{eq} .

As can be seen by comparing Figures 2 and 3, improv-

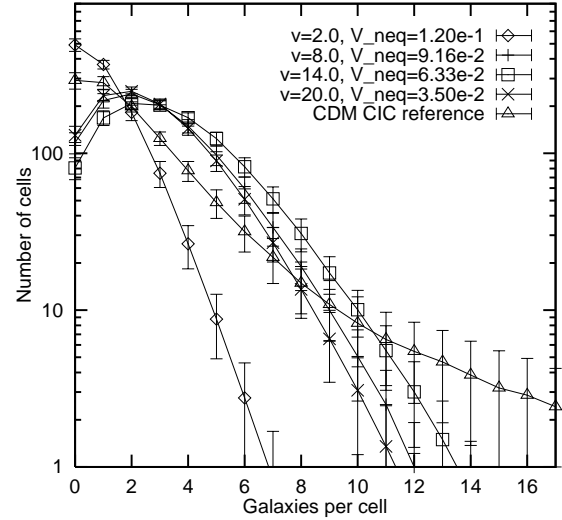


Figure 6. CIC statistics for different numbers $\nu = \nu_2$ of wakes per Hubble volume (ν). For comparison, the CDM curve is also shown. The variable V_{neq} is proportional to $G\mu$.

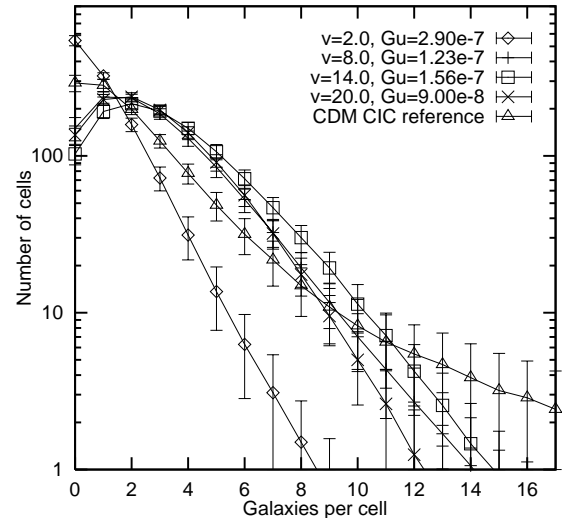


Figure 7. CIC statistics for different numbers of filaments per Hubble volume (ν). For comparison, the CDM curve is also shown.

ing the redshift accuracy for a fixed magnitude limit (which should be realized when the survey is complete) greatly improves the ability of the CIC statistic to discriminate between the different models. In this case, the texture, string and CDM models are all three clearly distinguishable. As an interesting side result, we note that the string filament and string wake models give almost identical results in spite of the radically different structure morphology they predict. Since it is unclear which of these string toy models corresponds more closely to an actual cosmic string model with HDM, the fact that they produce very similar CIC statistics is encouraging since it means that the uncertainty in the string evolution factors out.

Obviously, the power of the CIC to differentiate between the models also gets larger by increasing the limiting magnitude (which can be realized by using a larger telescope or by improving the sensitivity of the CCD cameras used). Fig-

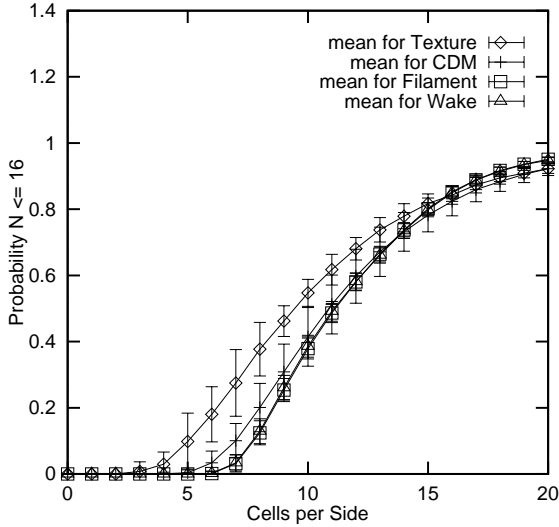


Figure 8. Cumulative NPF statistic (for $N < 17$) evaluated for the specifications of the UBC-NASA survey for the four models considered here. The horizontal axis is inversely proportional to the length of an individual sample volume.

ure 4 shows the results which can be obtained for limiting magnitude $R = 23$ and redshift error $\Delta z = 0.03$, Figure 5 depicts the results for the target values of the LZT project, $R = 23$ and $\Delta z = 0.01$.

Figures 6 and 7, respectively, show how the string wake and string filament curves vary when changing the parameters of the string models (the string filament and wake models of Figs. 2 - 5 were run for $\nu_2 = 10$). As the number ν_2 of structures per volume t^3 increases, the mass per unit length μ must be reduced if the total clustered mass is to remain the same. For comparison, the results for the standard CDM models are also depicted. It is obvious that changing the number ν_2 over one order of magnitude leads to a substantial change in the CIC curve. For a fixed number n of galaxies, the change in the amplitude of the CIC curves between the string results for $\nu_2 = 2$ and $\nu_2 = 20$ is comparable to the difference between the CDM and string curves. Nevertheless, we see by inspection that the shape of the string curves does not change substantially when ν_2 varies. Thus, by focusing on the shape of the CIC curves over the entire range of n rather than on the amplitude for fixed n , one can differentiate between the theories independent of the value of ν_2 . One way to quantify the information about the shape of the curve is to focus on its slope in the region between the value $n = n_{peak} + 2$ (where n_{peak} is the value of n corresponding to the peak of the CIC curve; the value $n_{peak} + 2$ was chosen in order to eliminate boundary effects at $n = 0$) and $n = n_{1/4}$ (where $n_{1/4}$ is the value of n at 1/4 the maximal height on the logarithmic plot). For simulations with $R = 23$ and $\Delta z = 0.01$, the slope varies between 0.94 and 0.51 in the string models, is about 0.31 in the CDM model and 0.11 in the texture theory.

As an interesting and unexpected side result of our study we mention the fact that for fixed value of ν_2 , the string filament and string wake curves are essentially indistinguishable. This implies that some of the uncertainties in the cosmic string theory of structure formation (see Section

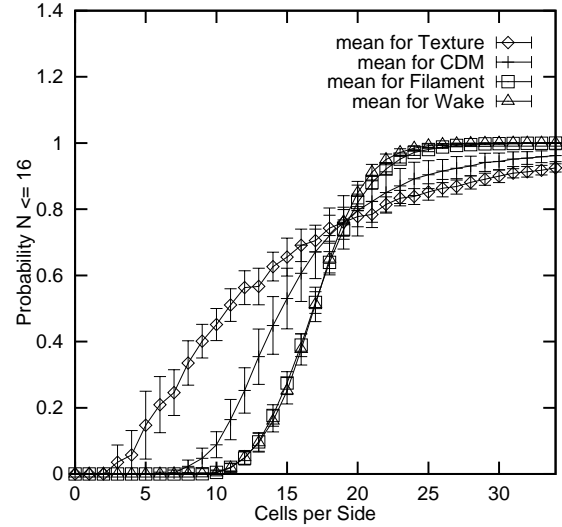


Figure 9. Cumulative NPF statistic (for $N < 17$) evaluated for the specifications of the LZT survey.

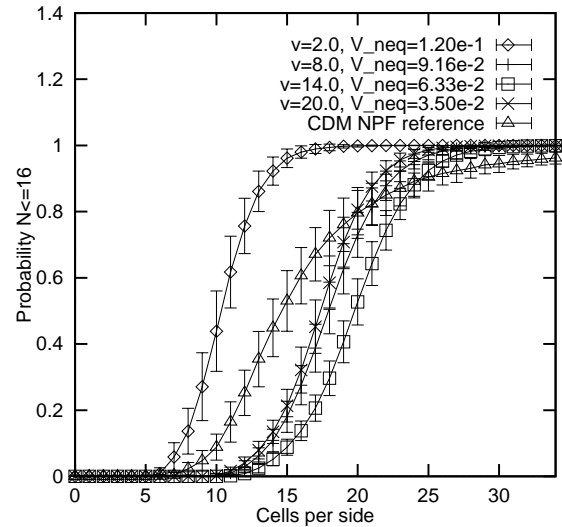


Figure 10. Cumulative NPF statistic (given the specifications of the previous figure) in the string wake model for different values of the number of wakes per Hubble volume.

2) cancel out when considering the CIC statistic, at least to the accuracy studied here.

The differences in the CDM, string and texture model CIC curves stem from the different morphologies which leads to different strengths of clustering on small scales. Since we model textures as spherically symmetric overdensities with a Gaussian density profile, there is a high degree of central clustering which leads to a large tail in the CIC curve. On the other hand, there are also large regions empty of galaxies which leads to the large peak at $n = 0$, where n is the number of galaxies per cell. In contrast, the string model leads to filamentary and planar clustering, and thus the predicted tail in the CIC curve is small. It is well known that nonlinear evolution (Gott et al. 1987, Park & Gott 1991) in the CDM model leads to a meat ball topology and hence to a significant tail in the CIC curve.

Figures 8 and 9 show the cumulative NPF statistic as a

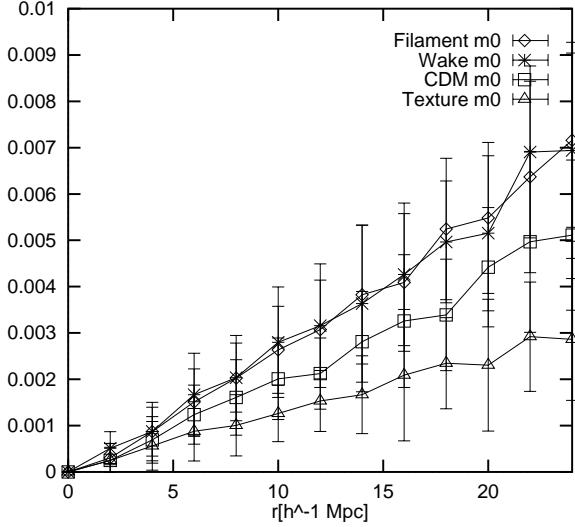


Figure 11. The Minkowski functional M_0 for a LMT survey with specifications $R = 20.4$ and $\Delta z = 0.01$. Note that the larger the value of r , the smaller the effective density threshold.

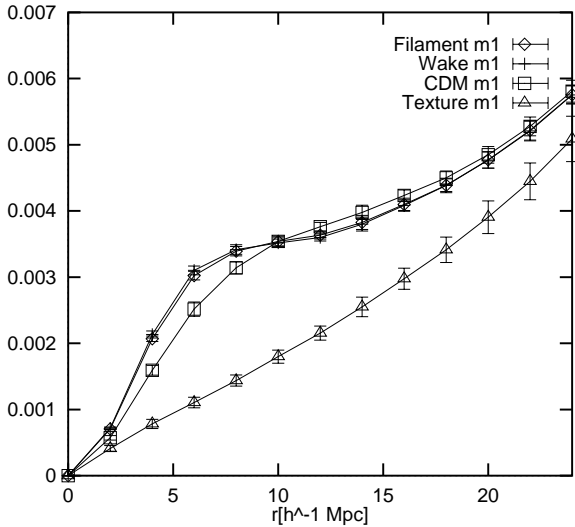


Figure 12. Same for M_1 .

function of radius for the specifications of the UBC-NASA and LZT surveys, respectively. The four curves represent the same four models for which the CIC statistics were shown in previous figures. The distinguishing power of the statistic was largest for the value $N = 16$, the value used in Figures 8 and 9. The conclusions are very similar to those obtained by means of the CIC statistic: with the specifications of the current UBC-NASA survey, the texture model can already be differentiated in a statistically significant way from the other models. Using conservative specifications of the LZT telescope currently under construction, the string, texture and CDM models all give very different curves. The string wake and string filament models remain indistinguishable. Figure 10 shows how the NPF changes as the number ν_2 of wakes per volume t^3 is varied (the simulations used for Fig. 10 are for the specifications of the LZT survey).

To obtain the best differentiation between the various models (independent of ν_2) it is again advisable to look at

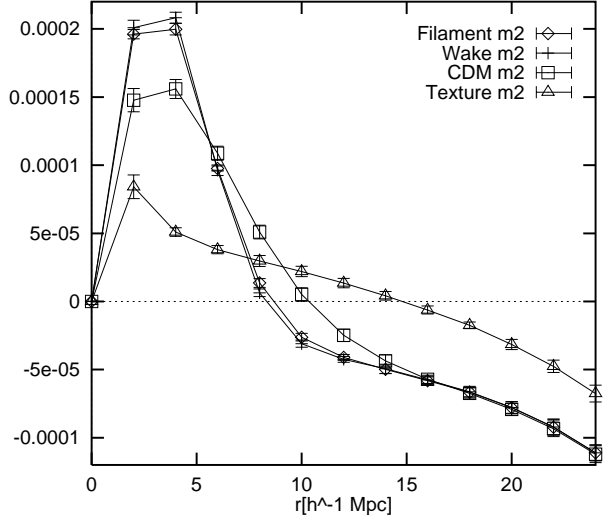


Figure 13. Same for M_2 .

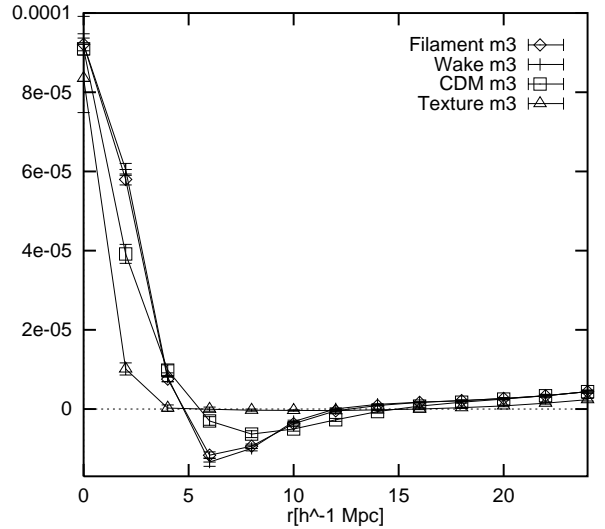


Figure 14. Same for M_3 .

the slope of the curve rather than at the amplitude for a fixed cell volume. The value of Δx (where x is the number of cells per side), which is a measure of the inverse of the slope, taken in the range over which the cumulative NPF increases from 0.2 to 0.8, varies between 4 and 5.7 for the string models, whereas it is approximately 8.7 for the CDM simulation and 15.5 for the texture model.

Figures 11 - 14 show the four Minkowski functionals $M_0 - M_3$ evaluated for all four models in the case of the specifications of the UBC-NASA survey with improved redshift errors ($R = 20.4$ and $\Delta z = 0.01$). The power of the functionals $M_1 - M_3$ (in particular M_1 and M_2) to differentiate between the models is comparable if not greater than the power of either the CIC or NPF statistics. In fact, using M_2 the UBC-NASA survey already offers the potential of separating the predictions of string, texture and CDM models.

5 DISCUSSION AND CONCLUSIONS

In this paper we have investigated the potential of the UBC-NASA and the LZT liquid mirror telescope redshift surveys to be able to differentiate between the predictions of various models of structure formation, in spite of the relatively large redshift uncertainties inherent to the survey strategy. We focused on the use of topological statistics to distinguish between models with identical power spectra but different phase structure, resulting in different morphology of the predicted large-scale structure in the Universe.

One of our main results is that the current UBC-NASA liquid mirror telescope survey will already be able to yield first interesting results. In particular, using counts in cell (CIC), N-galaxy probability functions and Minkowski functionals, the predictions of the texture model can be separated from those of other models with a high statistical significance. We have seen that an improvement in the redshift accuracy by a factor of 3 can yield a substantial increase in the ability of the survey to distinguish between different models. With the current limiting magnitude of $R = 20.4$ but with an improved redshift error of $\Delta z = 0.01$, the UBC-NASA survey will be able to yield results by means of which (making use of CIC, NPF and Minkowski functional statistics) the cosmic string models, texture models and standard CDM models can all be differentiated. In fact, the resolution power is larger than what can be achieved with $R = 23$ and $\Delta z = 0.03$. We have seen that with a survey having the target parameters of the LZT project ($R = 23$ and $\Delta z = 0.01$) a lot can be learned about the origin of structure in the Universe.

A very promising statistic appears to be M_2 , the third Minkowski functionals which measures the integrated mean curvature. With M_2 , the current UBC-NASA survey already has the potential of discriminating between string, texture and CDM models. It is interesting that M_2 appears to be a more powerful statistic than the widely used genus statistic M_3 .

There are, however, some important caveats concerning this study. The topological defect models we have analyzed are *toy models* and not actual simulations which include the complete nonlinear defect and gravitational dynamics (such simulations are at the moment out of the range of the capabilities). Our toy models are intended to capture the crucial morphological differences in the predicted large-scale structure between the models, differences which will be imprinted on the CIC, NPF and Minkowski functional statistics which are sensitive to the morphology of structure. Our defect toy models do not include any super-Hubble scale correlations. Neither do they include correlations of the defect distribution at different Hubble times (such correlations would be expected to be quite important in string models and probably less important in the texture model). We have neglected the effects of small-scale fluctuations (imprinted before t_{eq}) which can be very important (in particular in a cosmic string model with cold dark matter (Albrecht & Stebbins 1992)), and we have replaced the nonlinear dynamics of the structures seeded by an individual defect by an ad-hoc distribution of galaxies within these structures motivated by calculations using the Zel'dovich approximation, thus omitting extra nonlinear gravitational clustering. It would be interesting to redo the analyses of this paper using improved

simulations of defect models. It would also be interesting to study the potential of the LZT project to differentiate between the predictions of different CDM models (open CDM, Λ CDM, mixed dark matter models). Work on these issues is in progress.

Acknowledgments

We are grateful to Martin Götz for running the CDM simulation for us. We thank Ed Bertschinger for the use of his code (Bertschinger & Gelb 1991), Thomas Buchert and collaborators for making their Minkowski functional codes publically available, and Gerry Guralnik for granting us access to the computing facilities of the Brown Center for Scientific Computation. One of us (R.B.) wishes to thank Bill Unruh for hospitality at UBC in Vancouver over the period of several visits when some of the work reported here was carried out, and Martin Kerscher for comments on the draft. This work was supported in part by the U.S. Department of Energy under Contract DE-FG0291ER40688. D.M. was supported in part by a Brown University Royce Fellowship and by the NASA Space Grant Program. P.H. is supported by grants from the Natural Sciences and Engineering Research Council of Canada.

REFERENCES

- Aguirre, A., 1995, Senior thesis, Brown Univ. (unpublished).
Aguirre, A., & Brandenberger, R., 1995, Int. J. Mod. Phys., D4, 711; astro-ph/9505031.
Albrecht, A. & Stebbins, A., 1992, Phys. Rev. Lett., 68, 2121.
Albrecht, A. & Turok, N., 1989, Phys. Rev., D40, 973.
Allen, B. & Shellard, E.P.S., 1990, Phys. Rev. Lett., 64, 119.
Bardeen, J., Bond, J., Kaiser, N., & Szalay, A., 1986, Ap. J., 304, 15.
Bardeen, J., Steinhardt, P. & Turner, M., 1983, Phys. Rev., D28, 1809.
Bennett, D. & Bouchet, F., 1988, Phys. Rev. Lett., 60, 257.
Bertschinger, E. & Gelb, J., 1991, Computers in Physics, 5, 164.
Borra, E.F., Content, R., Girard, L., Szapitel, S., Tremblay, L.-M., & Boily, E., 1992, Ap. J., 393, 829.
Brandenberger, R., 1985, Rev. Mod. Phys., 57, 1.
Brandenberger, R., 1991, Phys. Scripta, T36, 114.
Brandenberger, R., 1994, Int. J. Mod. Phys., A9, 2117.
Brandenberger, R., Kaiser, N., Schramm, D. & Turok, N., 1987a, Phys. Rev. Lett., 59, 2371.
Brandenberger, R., Kaiser, N. & Turok, N., 1987b, Phys. Rev., D36, 2242.
Chibisov, G. & Mukhanov, V., 1980, 'Galaxy Formation and Phonons,' Lebedev Physical Institute Preprint No. 162.
Chibisov, G. & Mukhanov, V., 1982, MNRAS 200, 535.
Davis, R., 1987, Phys. Rev., D35, 3705.
de Lapparent, V., Geller, M. & Huchra, J., 1986, Ap. J. (Lett.), 302, L1.
Gooding, A., Spergel, D. & Turok, N., 1991, Ap. J. Lett., 372, L5.
Gott III, J.R., Weinberg, D. & Melott, A., 1987, Ap. J., 319, 1.
Guth, A. & Pi, S.-Y., 1982, Phys. Rev. Lett., 49, 110.
Hamilton, A., Saslaw, W. & Thuan, T., 1985, Ap. J., 297, 37.
Hawking, S., 1982, Phys. Lett. 115B, 295.
Hickson, P., Borra, E. F., Cabanac, R., Content, R., Gibson, B. K., & Walker, G. A. H., 1994, Ap. J., 436, L201.
Hickson, P., Borra, E. F., Cabanac, R., Chapman, S., de Lapparent, V., Mulrooney, M. & Walker, G. A. H., 1998, in Advanced Technology Optical/IR Telescopes VI, Proc. SPIE, 3352, in press.

- Hickson, P., Gibson, B. K. & Callaghan K., 1994, MNRAS, 267, 911.
- Hickson, P. & Mulrooney, M. K., 1998, Ap. J. (Suppl.), 115, 35.
- Hindmarsh, M. & Kibble, T.W.B., 1995, Rept. Prog. Phys., 58, 477.
- Kerscher, M. et al., 1997, MNRAS, 284, 73; astro-ph/9606133.
- Kibble, T.W.B., 1976, J. Phys., A9, 1387.
- Koo, D., 1985, Astron. J., 90, 418.
- Lanzetta, K., Yahil, A. & Fernandez-Soto, A., 1996, Nature, 381, 759.
- Leese, R. & Prokopec, T., 1991, Phys. Rev., D44, 3749.
- Lukash, V., 1980, Pis'ma Zh. Eksp. Teor. Fiz., 31, 631.
- Maddox, S., 1998, in Proceeding of Potsdam Cosmology Workshop "Large Scale Structure: Tracks and Traces", in press.; astro-ph/9711015.
- Mecke, K., Buchert, T. & Wagner, H., 1994, Astron. Astrophys. 288, 697.
- Mecke, K. & Wagner, H., 1991, J. Stat. Phys., 64, 843.
- Mukhanov, V. & Chibisov, G., 1981, JETP Lett., 33, 532.
- Park, C. & Gott III, J.R., 1991, Ap. J., 378, 457.
- Pen, U.-L., Seljak, U. & Turok, N., 1997, Phys. Rev. Lett., 79, 1611.
- Perivolarapoulos, L., Brandenberger, R. & Stebbins, A., 1990, Phys. Rev., D41, 1764.
- Press, W., 1980, Phys. Scr., 21, 702.
- Prokopec, T., 1991, Phys. Lett., 262B, 215.
- Saslaw, W., 1989, Ap. J., 341, 588.
- Schmalzing, J. & Buchert, T., 1997, Ap. J. (Lett.), 482, L1; astro-ph/9702130.
- Smoot, G. et al., 1992, Ap.J. (Lett.), 396, L1.
- Silk, J. & Vilenkin, A., 1984, Phys. Rev. Lett., 53, 1700.
- Starobinskii, A., 1982, Phys. Lett., 117B, 175.
- Turok, N., 1989, Phys. Rev. Lett., 63, 2625.
- Vilenkin, A., 1981, Phys. Rev., D23, 852.
- Vilenkin, A., 1985, Phys. Rep., 121, 263.
- Vilenkin, A. & Shafi, Q., 1983, Phys. Rev. Lett., 51, 1716.
- Vilenkin, A. & Shellard, E.P.S., 1994, Strings and Other Topological Defects. Cambridge Univ. Press, Cambridge.
- Zanchin, V., Lima, J.A.S., & Brandenberger, R., 1996, Phys. Rev., D54, 7219; astro-ph/9607062.
- Zel'dovich, Ya. B., 1970, Astron. Astrophys., 5, 84 (1970).
- Zucca, E. et al., 1997, Astron. Ap., 326, 477.